IEEE Access
Multidisciplinary | Rapid Review | Open Access Journal

Received 25 November 2024, accepted 18 December 2024, date of publication 23 December 2024,
date of current version 31 December 2024.

Digital Object Identifier 10.1109/ACCESS.2024.3521595

RESEARCH ARTICLE

Adaptive Semi-Supervised Fuzzy C-Means Method With Local Spatial Information and Pre-Clustering for Image Segmentation

HAO-RAN CHEN, XIAO-PENG WANG, JIA-XIN WU, AND HAI-ZHOU WANG
School of Electronic and Information Engineering, Lanzhou Jiaotong University, Lanzhou 730070, China
Corresponding author: Xiao-Peng Wang (wangxiaopeng@mail.lzjtu.cn)

This work was supported in part by the National Natural Science Foundation of China under Grant 61761027.

ABSTRACT The semi-supervised fuzzy C-means clustering algorithm is an improved version of the fuzzy C-means algorithm, designed to utilize a small amount of supervised information to enhance the clustering results. However, many semi-supervised fuzzy C-means algorithms suffer from the inadequate use of supervised information and sensitivity to noise. Therefore, this study employs pre-clustering and label propagation to enhance efficiency of supervision and introduces spatial information to improve the robustness of algorithm to noise. First, preliminary clustering of the supervised information is conducted to distinguish feature differences within each cluster, allowing the supervised information to guide clustering more rationally. Second, supervised information is disseminated to pixels with similar features, enabling a small amount of supervised information to guide the clustering process effectively. Then, an objective function with adaptive weights is designed to calculate the weights of the local spatial information and supervision weights based on the local spatial information and label spatial information respectively, enhancing the flexibility of algorithm. Finally, experimental results on synthetic images and multiple real image datasets demonstrate that the proposed algorithm can accomplish most segmentation tasks and, in most cases, outperforms other algorithms.

INDEX TERMS Fuzzy c-means, semi-supervised clustering, image segmentation, label propagation, local spatial information.

I. INTRODUCTION

The purpose of image segmentation is to divide images into meaningful regions based on attributes such as color and texture, which is a crucial topic in computer vision research. A wide array of image segmentation algorithms currently exists, including those based on thresholding [1], [2], edge detection [3], [4], [5], [6], morphology [7], [8], [9], [10], clustering [11], [12], [13], and deep learning [14], [15], [16]. Among these approaches, cluster analysis has long been a crucial tool in data analysis, aiming to group elements with similar characteristics into clusters, ensuring that the properties within a cluster are as similar as possible, whereas the properties between clusters are as distinct as possible. Such algorithms can also cluster image pixels based on their features, thereby achieving the goal of image segmentation. Image segmentation algorithms based on clustering are widely used because of their speed and high accuracy.

The Fuzzy C-Means (FCM) algorithm [17], based on the k-means algorithm, introduces the concept of fuzzy sets [18], using membership degrees to represent the weight of an element belonging to a particular cluster. This significantly enhances its flexibility compared to the k-means algorithm, making it a classic and robust method for image segmentation. However, image segmentation is a complex and uncertain problem, and relying solely on the information contained within an image makes accurate segmentation challenging for diverse image types. Fortunately, contextual information is available in many clustering application

The associate editor coordinating the review of this manuscript and approving it for publication was Ines Domingues.

scenarios. For example, using data from an imaging device or location can predetermine the clustering of certain pixels. Utilizing this information can improve the efficiency and accuracy of algorithms for extracting knowledge. Semi-supervised clustering segmentation algorithms [19], [20], [21], [22] have been designed precisely for such scenarios, incorporating a small amount of prior information from the image to guide the clustering process, thereby making the segmentation results more aligned with expectations. Pedrycz and Waletzky [23] first proposed a semi-supervised FCM algorithm, that incorporated a semi-supervised concept into FCM. Improvements to the semi-supervised FCM algorithm mainly focus on the following aspects: (1) Enhancing or expanding label forms. Peng et al. [24] proposed an algorithm that effectively leveraged pairwise constraint information. Antoine et al. [25] improved the Possibilistic Fuzzy C-Means (PFCM) clustering by using of a soft labeling mode, resulting in Semi-Supervised Possibilistic Fuzzy C-Means with Mahalanobis distance (SSPFCM) algorithm [26], better estimates cluster shapes and adapts to different data-labeling patterns. (2) Improving the supervision method. Yasunori et al. [27] introduced supervised membership into the semi-supervised FCM algorithm, eliminating the need for parameters to specify whether a pixel is labeled. Pedrycz et al. [28] introduced a regularization factor to balance the importance of the supervised and unsupervised information. Yin et al. [29] proposed an entropy-regularized semi-supervised fuzzy clustering algorithm that adaptively determined the fuzzy factor for different images. Bensaid et al. [30] first introduced the concept of a supervised center using supervised information to calculate the supervised center before the iteration begins, thereby strengthening the influence of supervised information on the clustering process. Semi-supervised clustering methods, while utilizing additional information such as labeled data, still fundamentally operate within the framework of unsupervised learning. These methods extract insights directly from the data without depending on a fully labeled dataset for training. In contrast, supervised methods are designed to apply learned knowledge to new, unlabeled data, a concept that is fundamentally different from semi-supervised clustering. This distinction results in differing problem formulations and solutions. The method explored in this paper, specifically within the context of image segmentation, does not align with learning-based supervised approaches. For a more comprehensive discussion on these differences, refer to the articles [31] and [32].

Although the semi-supervised FCM algorithm can enhance clustering performance, it still suffers from the same drawback as the FCM algorithm, namely its sensitivity to noise. When dealing with noisy images, algorithms often fail to produce satisfactory results. Various methods have been proposed to address the poor robustness of FCM algorithm: (1) Algorithms based on local spatial information. These algorithms improve segmentation results by correcting membership values using the statistical neighborhood information of pixels, such as FCM_S [33], FLICM [34], FCM_SICM [35], and RSFCM [36]. (2) Algorithms based on Non-local Spatial Information. These algorithms extract spatial information by identifying regions with similar characteristics in an image. Compared to local spatial information-based algorithms, non-local information can handle images heavily contaminated by noise. These algorithms primarily include FCM_NLS [37], FCM_SNLS [38], and FSC_LNML [39]. (3) Algorithms based on adaptive fuzzy spatial relations consider spatial relationships between pixels and their neighboring pixels. This approach effectively reduced the impact of noise on the clustering results and enhanced the spatial continuity of the image. These algorithms include GSFCM [40], RSSFCA [41], and ASWFCM [42]. (4) Algorithms incorporating various mathematical techniques. These methods use a range of mathematical techniques to extract and use information from images for segmentation. These algorithms include methods that combine Kullback-Leibler (KL) divergence, morphological reconstruction, and sparse representation. For example, Gharieb et al. [43] modified the objective function using KL divergence; and the FDCM algorithm [44] introduced sparse representation. The SPFCM algorithm [45] further integrated morphological grayscale reconstruction (MGR) with tight wavelet frame transform to enhance robustness. The aforementioned improved algorithms enhance the robustness of the FCM algorithm. However, within semi-supervised FCM algorithms, enhancements that leverage spatial information are relatively uncommon.

The above algorithms have inherent limitations. The semi-supervised FCM algorithm introduces a supervised regularization term into the objective function, enabling supervised information to impact clustering outcomes positively. However, this term typically includes only a small number of supervised pixels, thereby exerting limited influence on the vast majority of unlabeled pixels. Additionally, such algorithms require the specification of parameters for the regularization term and apply the same parameters to all pixels, thereby reducing their adaptability to diverse datasets and possibly introducing clustering inaccuracies. Methods based on local spatial information can enhance noise resistance but may compromise image detail when spatial information is directly used for clustering. Non-local information-based algorithms, on the other hand, experience greater computational demands as noise density rises. Moreover, if noise disrupts multiple similar regions, segmentation outcomes may still be suboptimal. Algorithms utilizing adaptive fuzzy spatial information dynamically adjust fuzzy factors or weight parameters according to image characteristics, thereby ensuring stable performance in diverse image segmentation tasks. However, these algorithms are highly sensitive to parameter selection, which complicates the parameter tuning process. Furthermore, in scenarios with non-uniform illumination or severe occlusion, excessive membership ambiguity may arise, adversely affecting segmentation outcomes.

In summary, the semi-supervised FCM algorithm retains limitations when processing noisy images. To improve its performance in noisy image segmentation, this study explores three key directions for enhancing the algorithm's performance: (1) insufficient utilization of supervised information. Due to the simplistic approaches employed in utilizing supervised information, the information contained in the labels is not fully discovered and utilized, leading to clustering results that deviate from supervised information. (2) Supervised weights often need to be manually selected and remain constant during the computational process, resulting in a lack of flexibility in the algorithm. (3) Semi-supervised fuzzy clustering suffers from the same noise sensitivity issue as FCM, and in semi-supervised fuzzy clustering, noise can contaminate the supervised information, thereby causing a more severe impact on the algorithm's performance.

To address the issues mentioned above, a Semi-supervised Fuzzy C-means Method with Local Spatial Information and Pre-clustering (SSFCM-LP) algorithm is proposed, presenting the following enhancements to the semi-supervised FCM algorithm: (1) Enhanced utilization of supervised information: To optimize the use of supervised information and enhance its efficacy in guiding clustering, a label propagation process is first applied, wherein the label information from labeled pixels is extended to all unlabeled pixels. This expands the influence range of supervised information. Subsequently, a pre-clustering process is performed on the supervised information to refine the clusters, enhancing cluster compactness and improving segmentation precision. (2) Dynamic parameter adjustment: To overcome the limitations of static parameterization, the algorithm leverages the spatial information of labeled pixels to evaluate label reliability and automatically determines the supervision strength of each pixel for each cluster. This approach enhances the algorithm's flexibility, ensuring greater adaptability to diverse scenarios. (3) Improved noise robustness: To bolster the algorithm's resistance to noise without significantly increasing computational complexity, local spatial information is incorporated into the algorithm. An adaptive coefficient controls the weights between the original information and local spatial information. Additionally, to address perceptual inconsistencies in the RGB color space, all image processing is conducted in the CIE Lab color space. These enhancements collectively address the limitations of the traditional semi-supervised FCM algorithm, enhancing its effectiveness and adaptability for noisy image segmentation tasks.

The remainder of this paper is structured as follows: Section II introduces the FCM clustering algorithm and a semi-supervised FCM algorithm; Section III explains the principles and details of the proposed algorithm; Section IV presents and discusses the experimental results of the algorithm on both synthetic and natural images; and Section V provides the conclusion.

II. RELATED WORK

A. SEMI-SUPERVISED ENTROPY REGULARIZED FUZZY C-MEANS CLUSTERING ALGORITHM

To improve the accuracy of FCM segmentation, Yasunori et al. introduced a correction term into the objective function of FCM clustering. Under the premise of knowing the categories of certain pixels, i.e., including labeled data, they proposed the Semi-Supervised Entropy Regularized Fuzzy C-Means Clustering algorithm (eSFCM) [27]. Its objective function and constraint condition are as follows:

$$J_{eSFCM} = \sum_{j=1}^{N}\sum_{i=c}^{k} u_{ij}\left\|x_j - c_i\right\|^2 + \lambda^{-1}\sum_{j=1}^{N}\sum_{i=1}^{k}\left|u_{ij} - \bar{u}_{ij}\right|\ln\left|u_{ij} - \bar{u}_{ij}\right| \quad (1)$$

$$s.t.\sum_{i=1}^{k} u_{ij} = 1, j = 1, 2, \ldots, N \quad (2)$$

where $X = \left\{x_1, x_2, \cdots, x_j, \cdots, x_N\right\}$ represents a dataset with N data points, k denotes the number of target clusters, u_{ij} represents the membership degree of the j-th data point to the i-th cluster, and $u_{ij} \in [0, 1]$; c_i denotes the cluster center of the i-th cluster; $\|\bullet\|^2$ denotes the squared Euclidean norm. λ represents the weight of supervision and $\bar{u}_{ij}$ denotes the supervised membership degree of the j-th data point to the i-th cluster. When the j-th data point is labeled as belonging to the i-th cluster, $\bar{u}_{ij} = 1$; otherwise, $\bar{u}_{ij} = 0$.

Using the constraint conditions and Lagrange multiplier method to minimize the objective function, the iterative formulas for u_{ij} and c_i are derived as follows:

$$u_{ij} = \bar{u}_{ij} + \frac{1 - \sum_{r=1}^{k}\bar{u}_{rj}}{\sum_{r=1}^{k} e^{-\lambda\|x_j - c_r\|^2}} e^{-\lambda\|x_j - c_i\|^2} \quad (3)$$

$$c_i = \frac{\sum_{j=1}^{N} u_{ij}x_j}{\sum_{j=1}^{N} u_{ij}}. \quad (4)$$

B. BILATERAL FILTERING

Traditional methods for obtaining spatial information typically consider only the relationship between a target pixel and its surrounding pixels, as exemplified by Gaussian filters. However, bilateral filtering [35] takes into account both spatial positional relationships and pixel color differences. This achieves different filtering effects in smooth areas and regions with large gradients, thereby preserving the edge details of an image. The equation for bilateral filtering is as

follows:

$$\omega(i,j,p,q) = \exp\left[-\frac{(i-p)^2+(j-q)^2}{2\sigma_d^2} - \frac{\|I(i,j)+I(p,q)\|^2}{2\sigma_r^2}\right] \tag{5}$$

$$I_D(i,j) = \frac{\sum_{p,q} I(p,q)\,\omega(i,j,p,q)}{\sum_{p,q}\omega(i,j,p,q)} \tag{6}$$

where σ_d and σ_r represent the geometric spread and photometric spread respectively; $I_D(i,j)$ denotes the filtered result; $I(i,j)$ and $I(p,q)$ represent the values of pixels (i,j) and (p,q) in the original image, with pixel (p,q) being a neighboring pixel in the window around pixel (i,j).

III. METHOD AND MOTIVATION

A. PRE-CLUSTERING OF SUPERVISED INFORMATION

Clustering segmentation typically requires the specification of the number of clusters. However, the specified number of clusters may not always correspond to the inherent features within the data, which often leads to a decline in algorithm performance. In such cases, subdividing the clusters can yield better segmentation results. For example, as illustrated in Fig. 1, two colors represent two types of data, with corresponding-colored circles indicating the range covered by the respective clusters during the clustering process. When the target number of clusters is set to two, the circles fail to precisely encompass each type of data, and the overlapping areas of the circles indicate regions that simultaneously belong to multiple clusters, resulting in a high probability of incorrect cluster assignment, as shown in Fig. 1(a). However, by subdividing one of the types into smaller subclasses, the overlapping areas between clusters are reduced, thereby improving clustering accuracy, as shown in Fig. 1(b).

This scenario is quite common in natural image pixels, particularly in images with uneven lighting or shadows. In such images, the pixel colors often follow this distribution. Fig. 2(a) depicts an image of a chair with sunlight and shadows that can be segmented into two regions, while the background and shadow regions form elongated shapes as shown in Fig. 2(b). If the original image is segmented directly, the clustering ranges of the two regions will overlap significantly, leading to large areas of error in the segmentation result, as illustrated in Fig. 2(c). However, by dividing the background into two subclasses, dark and light, and then clustering, the overlap in the clustering ranges can be significantly reduced. After segmentation, merging all subclasses to obtain the final segmentation result can improve accuracy, as shown in Fig. 2(d) and Fig. 2(e).

When dealing with images containing more complex objects or backgrounds, manually determine reasonable subcategories becomes increasingly challenging, as demonstrated in the example above. In the unsupervised FCM algorithm, addressing this issue is often challenging. However, in the semi-supervised FCM algorithm, this paper utilizes semi-supervised information to pre-cluster the supervision data associated with each class. By refining the features incorporated into the semi-supervision, the number of features within each subclass cluster is reduced, thereby aiding the clustering process in forming mean regions. Ultimately, the algorithm reassembles the contiguous areas of subclasses, thereby enhancing overall segmentation performance.

In this study, the supervision information for each category is clustered using the density peaks (DP) clustering method [46], and the supervision information is divided into subcategories according to the clustering results. Since semi-supervised information may inherently be contaminated by noise, the DP algorithm might select erroneous data points as cluster centers. The clustering results of DP are highly dependent on the selection of these cluster centers, which can lead to significant clustering errors, known as the domino effect [47]. Therefore, this study accounts for all pixels within the neighborhood window of each labeled pixel to calculate the local density, thereby reducing the impact of noise on pre-clustering.

First, calculate the local density ρ for the supervised data labeled as belonging to the ith class:

$$\rho_l = \sum_{l\neq j} e^{-\left[\frac{|x_l-I_l|}{d_{\text{cut}}}+\left(\frac{d_{lj}}{d_{\text{cut}}}\right)^2\right]} \tag{7}$$

where d_{lj} represents the distance between the l-th supervised data and the j-th data. d_{cut} denotes the cutoff distance, a parameter specified in advance. x_l indicates the pixel value of the l-th pixel. I_l represents the average value of the neighboring pixels around the l-th pixel. When the j-th pixel is contaminated by noise, its difference from the surrounding pixels increases, thereby reducing the local density of the j-th pixel and decreasing its likelihood of being selected as a cluster center.

Let δ_l represent the distance between the data point l and the nearest data point with a higher local density:

$$\delta_l = \min_{j:\rho_j>\rho_l} d_{lj}. \tag{8}$$

For any labeled data point l, the most probable cluster centers can be identified based on two quantities: ρ_l and δ_l. A cluster center should have a high local density and be far from points with a higher density, meaning it should have large values for both ρ_l and δ_l. Let $\gamma_l = \rho_l \times \delta_l$, if $\gamma_l > d_{cut}$, the data point is selected as a cluster center. Noncentrality data points wrer assigned to the same cluster as their nearest cluster center. According to the pre-clustering results, the number of target clusters used in the main clustering process can be obtained as follows:

$$\tilde{k} = \sum_{i=1}^{k} s_i \tag{9}$$

where s_i denotes the number of subclasses belonging to the ith class. Additionally, the pre-clustering results of the labeled data belonging to the i-th class, denoted

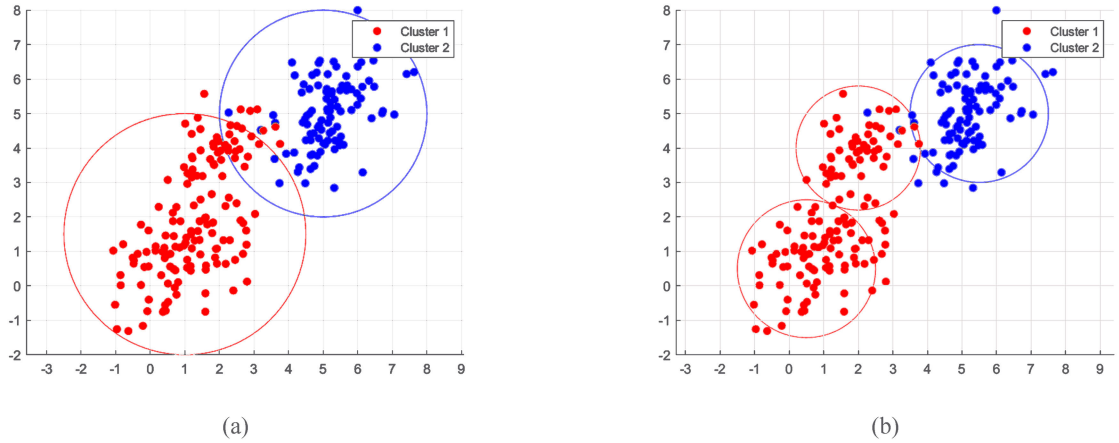

FIGURE 1. The influence of pre-clustering on the range of class clusters. (a)Cluster without pre-clustering. (b)Cluster with Pre-clustering.

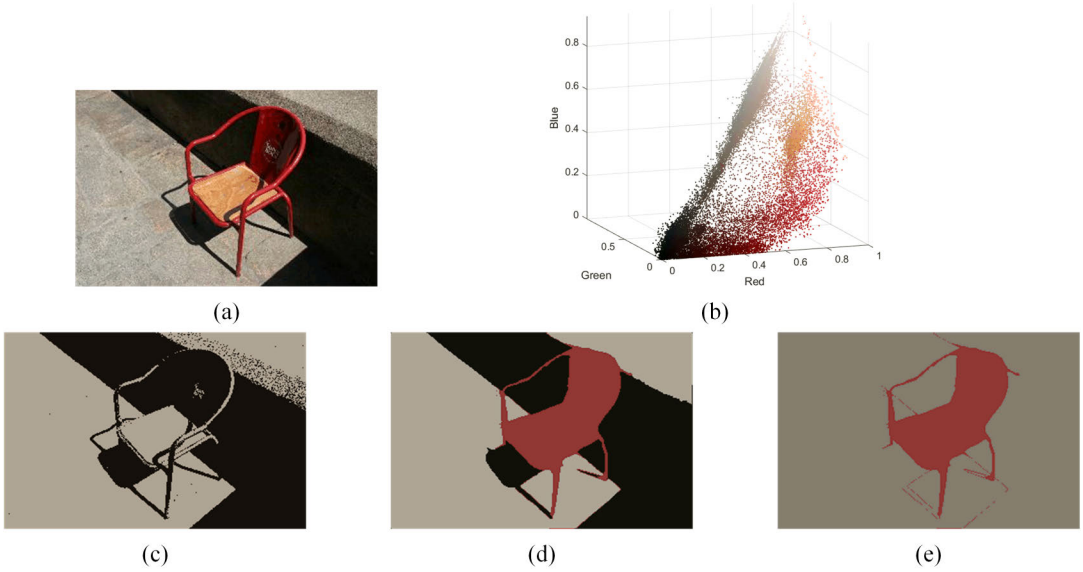

FIGURE 2. The influence of subclasses on image segmentation. (a) Original image. (b) Pixel color distribution of (a). (c) The segmentation result without subclasses. (d) The segmentation result of subclasses. (e) The segmentation result with subclasses.

as $\{X_{i1}, X_{i2}, \cdots, X_{is_i}\}$, become the supervision information for the corresponding actual clusters. After this step, the original clusters are refined into more subclasses, with each subclass possessing its own supervised information.

The selection of the parameter d_{cut} in pre-clustering significantly influences the number of generated subclasses, thereby directly affecting the algorithm's accuracy and runtime. Therefore, careful consideration must be given to its selection. Fig. 3 illustrates the impact of varying d_{cut} values on the algorithm's performance within the Berkeley dataset [48]. The figure primarily displays the algorithm's runtime alongside normalized evaluation metrics (where the peak signal-to-noise ratio is normalized within the 0-30 dB range), with detailed explanations of these metrics provided in Section IV-A. From Fig. 3, it is evident that when d_{cut} is less than 10, the evaluation metrics exhibit only slight fluctuations, whereas the runtime remains comparatively long. As d_{cut} increases, the algorithm's runtime decreases; however, significant declines in the evaluation metrics occur only when d_{cut} exceeds 20. This is because the generated subclasses fail to capture the main features of the image. Fig. 4 and Fig. 5 present the segmentation results for two natural images from the Berkeley dataset, with the first row depicting the segmentation outcomes for various d_{cut} values and the second row illustrating the final results after merging the corresponding subclasses. The conclusions drawn from Fig. 4 and Fig. 5 are consistent with the observed performance of the data. When d_{cut} is small, the segmentation results remain largely unchanged; however, when d_{cut} is excessively large, incorrect segmentation occurs, particularly in the yellow regions of the background (as illustrated in Fig. 4(m) and (n)). Fig. 5 also demonstrates similar segmentation

errors resulting from a high cutoff distance, as illustrated in Fig. 5(n).

Experimental results indicate that selecting d_{cut} values ranging from 10 to 15 optimally balances performance and runtime across most images. To prevent abrupt declines in algorithm performance resulting from d_{cut} selection and to more clearly illustrate the effects of pre-clustering, a value of 10 will be employed for this parameter in the subsequent sections of this paper.

The pre-clustering process integrates a divide-and-conquer strategy into the FCM image segmentation method by decomposing complex and challenging segmentation tasks into multiple homogeneous sub-tasks based on semi-supervised information. This approach simplifies the identification of regions with distinct features, making them more manageable. Furthermore, it extends the utility of semi-supervised information, enabling it to guide the iterative process while also influencing the dimensionality of the supervision matrix. This dual role allows for a more thorough extraction and utilization of the inherent value in semi-supervised information.

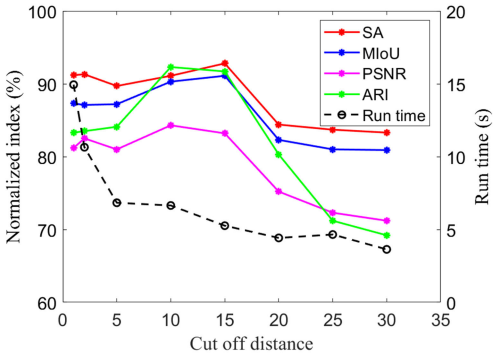

FIGURE 3. Normalized index (%) and run time (s) of the algorithm with different dcut on Berkeley database.

B. METHOD FOR FILLING SUPERVISED MEMBERSHIP MATRIX

In the semi-supervised FCM algorithm, supervised information influences and directs the clustering process in the form of a supervision matrix within the objective function. One method for constructing the supervision matrix is as follows: if the l-th pixel in the image is assigned to the i-th class, then its supervised membership for the i-th class is 1, and for other classes, it is 0. However, because of the high cost of labeling or the limited availability of labeled data in some cases, most pixels cannot be labeled. Therefore, the initial supervision matrix often contains numerous missing values, denoted as NA. For example:

$$\begin{pmatrix} NA & NA & NA & \cdots & NA \\ 0 & 0 & 1 & \cdots & 0 \\ NA & NA & NA & \dots & NA \\ \vdots & \vdots & \vdots & \vdots & \vdots \\ NA & NA & NA & \dots & NA \end{pmatrix}_{N\times\tilde{k}}. \tag{10}$$

By assigning a value of zero to the missing entries, calculations can proceed, however, at this point, the supervision information might be too sparse to effectively guide the clustering process, leading to unsatisfactory clustering results. As shown in Fig. 6(b), there is a group of supervision information within the red rectangle, but the segmentation result for the pixels neighboring the labeled pixel is not influenced by this supervision information, as illustrated in Fig. 6(c). To ensure that the clustering results align with supervision information, alternative methods should be employed to fill the missing values in the matrix.

The missing values of matrix should be filled based on the following principles: (1) Color consistency principle: If an unlabeled pixel has an identical color to a labeled pixel, the unlabeled pixel should have the same supervised membership as the labeled pixel. (2) Maximum color difference principle: If the color difference between an unlabeled pixel and any labeled pixel is the greatest among all the pixel color differences in the image, the supervised membership of the unlabeled pixel to the same class as the labeled pixel should be zero. Given these principles, and considering that pre-clustering ensures no significant differences within the same class of supervision information, and to optimize the algorithm runtime, only the supervision information with the smallest spatial distance to each pixel within the same class will be considered when filling missing values.

The method for calculating the supervised membership of the j-th unlabeled pixel to the i-th class is as follows:

$$\tilde{u}_{ij} = 1 - \frac{\Delta E_{ij}}{\Delta E_{max}} \tag{11}$$

where ΔE_{ij} represents the color difference between the j-th unlabeled pixel and the nearest labeled pixel belonging to the i-th class. ΔE_{max} denotes the maximum color difference among all pixels in the image. However, calculating ΔE_{max} has high computational complexity, making it difficult to obtain for larger images. Therefore, the maximum color difference between the labeled pixels, $\Delta \bar{E}_{max}$, can be used as a substitute for ΔE_{max}. Thus, we obtain the following supervised membership matrix:

$$\begin{aligned} \mathbf{F} &= \begin{pmatrix} F_{11} & F_{21} & F_{31} & \cdots & F_{c1} \\ F_{12} & F_{22} & F_{32} & \cdots & F_{c2} \\ F_{13} & F_{23} & F_{33} & \dots & F_{c3} \\ \vdots & \vdots & \vdots & \vdots & \vdots \\ F_{N1} & F_{N2} & F_{N3} & \dots & F_{Nc} \end{pmatrix}_{N\times\tilde{k}} \\ &= \begin{pmatrix} \tilde{u}_{11} & \tilde{u}_{21} & \tilde{u}_{31} & \cdots & \tilde{u}_{c1} \\ 0 & 0 & 1 & \cdots & 0 \\ \tilde{u}_{13} & \tilde{u}_{23} & \tilde{u}_{33} & \dots & \tilde{u}_{c3} \\ \vdots & \vdots & \vdots & \vdots & \vdots \\ \tilde{u}_{N1} & \tilde{u}_{N2} & \tilde{u}_{N3} & \dots & \tilde{u}_{Nc} \end{pmatrix}_{N\times\tilde{k}}. \end{aligned} \tag{12}$$

Through label propagation, label information diffuses across the entire image. During the iterative process, label information not only indirectly influences other pixels, as seen in traditional semi-supervised methods, but also

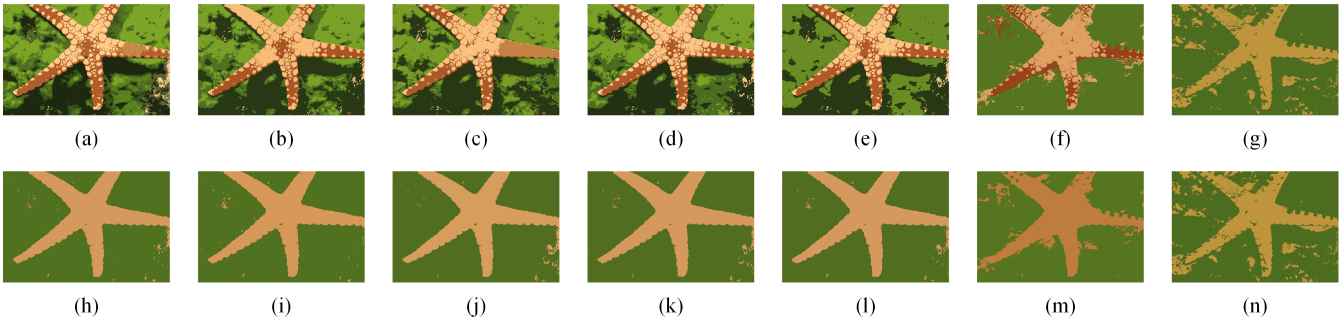

FIGURE 4. Pre-clustering and segmentation results on #12003 with different d_{cut}. (a)-(g) Pre-clustering result. (h)-(n) Segmentation results. (a) and (h) $d_{cut} = 1$. (b) and (i) $d_{cut} = 2$. (c) and (j) $d_{cut} = 5$. (d) and (k) $d_{cut} = 10$. (e) and (l) $d_{cut} = 15$. (f) and (m) $d_{cut} = 20$. (g) and (n) $d_{cut} = 25$.

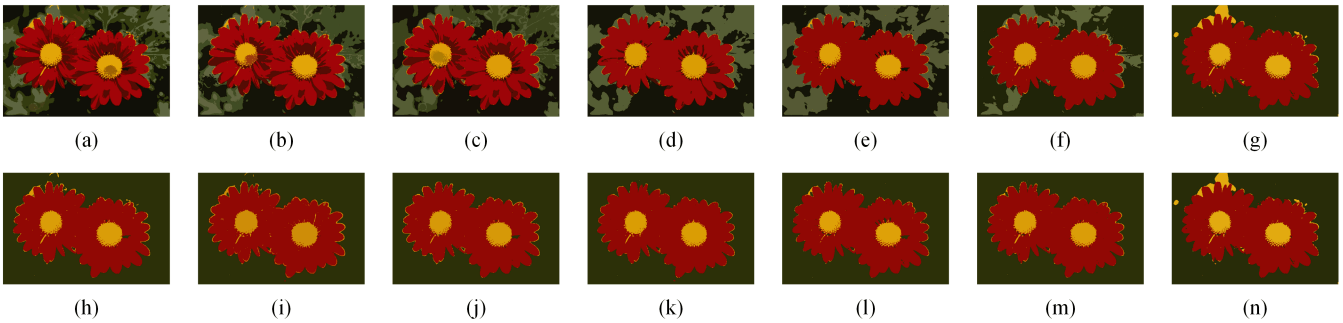

FIGURE 5. TPre-clustering and segmentation results on #124084 with different d_{cut}. (a)-(g) Pre-clustering result. (h)-(n) Segmentation results. (a) and (h) $d_{cut} = 1$. (b) and (i) $d_{cut} = 2$. (c) and (j) $d_{cut} = 5$. (d) and (k) $d_{cut} = 10$. (e) and (l) $d_{cut} = 15$. (f) and (m) $d_{cut} = 20$. (g) and (n) $d_{cut} = 25$.

FIGURE 6. The influence of label propagation. (a)Original image. (b) Segmentation result without label propagation. (c)A set of labeled pixels and their neighborhoods.

directly guides the clustering of all pixels. This dual influence enhances the algorithm's generalization ability and improves the overall utilization of the data. Subsequent experiments demonstrate that, following label propagation, the clustering segmentation results no longer exhibit the issues shown in Fig. 6(b) and Fig. 6(c).

C. SSFCM-LP

1) OBJECTIVE FUNCTION

The objective function of SSFCM_LP consists of an unsupervised part J_o and a supervised part J_s:

$$J = J_o + J_s. \tag{13}$$

A supervision weight matrix is incorporated into the objective function to balance the credibility of the propagated supervision information. This matrix assigns different supervision weights to each pixel, where A_{ij} represents the supervision weight of the j-th pixel in the i-th cluster. The two components of the objective function are defined as follows:

$$J_o = \sum_{i=1}^{\tilde{k}} \sum_{j=1}^{N} \left(1 - A_{ij}\right) u_{ij}{}^2 \left(\alpha \left\|x_j - c_i\right\|^2 + \beta \left\|\bar{x}_j - c_i\right\|^2\right) \tag{14}$$

$$J_s = \sum_{i=1}^{\tilde{k}} \sum_{j=1}^{N} A_{ij} \left(u_{ij} - F_{ij}\right)^2 \left[\alpha \left(\left\|x_j - c_i\right\|^2 + \left\|x_j - \bar{c}_i\right\|^2\right) + \beta \left(\left\|\bar{x}_j - c_i\right\|^2 + \left\|\bar{x}_j - \bar{c}_i\right\|^2\right)\right] \tag{15}$$

where x_j denotes the j-th pixel in the original image, and $\bar{x}_j$ represents the j-th pixel after processing the original image by using (6). The objective function involves two sets of

parameters: supervision matrix $\mathbf{A}$, which controls the strength of supervision, and parameters α and β, which control the intensity of the local spatial information. Additionally, to enhance the influence of supervision information on clustering, a supervision center $\bar{c}_i$ was introduced [49].The choices of these parameters and the calculation of the supervision center are discussed in the next subsection.

2) PARAMETERS SELECTION AND SUPERVISED CENTER

Parameters α and β control the intensity of local spatial information in the objective function. Literature [35] provides a method for calculating the weights α and β:

$$\alpha = \frac{1}{\left|x_j - \bar{x}_j\right| + \text{eps}} \tag{16}$$

$$\beta = \left|x_j - \bar{x}_j\right| + \text{eps} \tag{17}$$

where eps is a sufficiently small number that prevents the denominator from becoming zero. The more severely pixel x_j is corrupted by noise, the greater the $\left|x_j - \bar{x}_j\right|$, that is, the greater the intensity difference between the original pixel and the bilaterally filtered pixel. Consequently, the segmentation result should be influenced more by the bilaterally filtered image (requiring a larger β) and less by the original image (requiring a smaller α). Conversely, when the effect of noise is minimal, the original image should have a greater influence on preserving the original information.

The parameter matrix $\mathbf{A}_{N\times\tilde{k}}$ controls the extent to which the pixel clustering is influenced by the supervision matrix. The elements of the supervision intensity matrix $\mathbf{A}$ are obtained using the following method:

$$A_{ij} = \frac{d_{ij_{min}}^{-1}}{\sum_{r=1}^{\tilde{k}} d_{rj_{min}}^{-1}} \tag{18}$$

where $d_{ij_{\min}}$ represents the distance from the j-th pixel to the nearest supervised pixel belonging to the i-th cluster; A_{ij} denotes the supervision weight of the j-th pixel for the i-th cluster. Since most of the supervision information is obtained through label propagation, and this information does not consider spatial information and may not always be accurate, it is necessary to assign parameters to these pixels to measure the influence of the propagated label data on clustering. When a pixel is far from any supervised pixel, it is less influenced by the supervision information during the clustering process. Conversely, when a pixel is close to particular supervision information, it receives a greater supervision intensity for that cluster.

To enhance the impact of supervision information on clustering, the supervision center for each subcategory is calculated and integrated into the objective function. The supervision center is computed using the weighted average of the original image and spatial information, thereby avoiding significant deviations caused by the contamination of the supervision pixels. The calculation method is as follows:

$$\bar{c}_i = \frac{\sum_{j=1}^{N} F_{ij}^2 \left(\frac{\alpha x_j + \beta \bar{x}_j}{\alpha+\beta}\right)}{\sum_{j=1}^{N} F_{ij}^2} = \frac{\sum_{j=1}^{N} F_{ij}^2 \left(\alpha x_j + \beta \bar{x}_j\right)}{(\alpha+\beta)\sum_{j=1}^{N} F_{ij}^2}. \tag{19}$$

This method ensures that the supervision center accurately reflects the distribution of the original and spatially weighted information, thus providing a robust guide for the clustering process.

3) ITERATION FORMULA CALCULATION

First, to make subsequent expressions more concise and intuitive, the unsupervised center distance D and supervised center distance $\bar{D}$ are defined as follows:

$$D = \alpha \left\|x_j - c_i\right\|^2 + \beta \left\|\bar{x}_j - c_i\right\|^2 \tag{20}$$

$$\bar{D} = \alpha \left(\left\|x_j - c_i\right\|^2 + \left\|x_j - \bar{c}_i\right\|^2\right) + \beta \left(\left\|\bar{x}_j - c_i\right\|^2 + \left\|\bar{x}_j - \bar{c}_i\right\|^2\right). \tag{21}$$

Next, the Lagrange multiplier method is used to minimize the objective function and solve for the membership matrix and cluster centers. The Lagrangian function J_λ is as follows, where λ_j is the Lagrangian factor:

$$J_\lambda = J + \sum_{j=1}^{N} \left[\lambda_j \left(\sum_{i=1}^{\tilde{k}} u_{ij} - 1\right)\right]. \tag{22}$$

Then derive the expression for u_{ij}:

$$\begin{aligned} &\frac{\partial J_\lambda}{\partial u_{ij}} = 0 \\ &\Rightarrow 2\left(1 - A_{ij}\right) u_{ij} D + 2A_{ij}\left(u_{ij} - F_{ij}\right)\bar{D} + \lambda_j = 0 \\ &\Rightarrow u_{ij} = \frac{A_{ij}F_{ij}\bar{D} - \frac{\lambda_j}{2}}{\left(1 - A_{ij}\right) D + A_{ij}\bar{D}}. \end{aligned} \tag{23}$$

Substitute (23) into constraint condition $\sum_{i=1}^{\tilde{k}} u_{ij} = 1$:

$$\begin{aligned} &\sum_{i=1}^{\tilde{k}} \frac{A_{ij}F_{ij}\bar{D} - \frac{\lambda_j}{2}}{\left(1 - A_{ij}\right) D + A_{ij}\bar{D}} = 1 \\ &\Rightarrow -\frac{\lambda}{2} = \frac{1 - \sum_{i=1}^{\tilde{k}} \frac{A_{ij}F_{ij}\bar{D}}{(1-A_{ij})D + A_{ij}\bar{D}}}{\sum_{i=1}^{\tilde{k}} \left[\left(1 - A_{ij}\right) D + A_{ij}\bar{D}\right]^{-1}}. \end{aligned} \tag{24}$$

Let $w_{ij} = \left(1 - A_{ij}\right) D + A_{ij}\bar{D}$ and substitute (24) into (23):

$$u_{ij} = \frac{A_{ij}F_{ij}\bar{D} + \frac{1 - \sum_{r=1}^{\tilde{k}} \frac{A_{rj}F_{rj}\bar{D}}{w_{rj}}}{\sum_{r=1}^{\tilde{k}} w_{rj}^{-1}}}{w_{ij}}$$

$$= \frac{A_{ij}F_{ij}\bar{D}}{w_{ij}} + \frac{1 - \sum_{r=1}^{\tilde{k}} \frac{A_{rj}F_{rj}\bar{D}}{w_{rj}}}{\sum_{r=1}^{\tilde{k}} w_{rj}^{-1}} w_{ij}^{-1}. \quad (25)$$

Next, derive the expression for c_i using (26), as shown at the bottom of the next page.

By updating u_{ij} and c_i using (25) and (26), the objective function can be minimized. Finally, each pixel is applied to the cluster with the highest membership value, and the implementation steps of SSFCM-LP are as follows:

INPUT: Number of clusters k, noisy image I_n, supervision information F, maximum number of iterations $iter_{max}$, minimum error ε.

Step 1: Compute filtered image using (5) and (6).
Step 2: Convert the color system of the image to CIE Lab.
Step 3: Cluster the supervision information for each cluster using (7) to (8), and the number of subclasses $\tilde{k}$ using (9).
Step 4: Compute the supervised membership matrix $\mathbf{F}$ using (11) and (12).
Step 5: Compute the supervision intensity matrix $\mathbf{A}$ using (18) and supervised center $\bar{c}$ using (19).
Step 6: Initialize the membership matrix $\mathbf{U}$ using the normalized supervised membership matrix $\mathbf{F}$.
Step 7: $iter = 0, J^{(0)} = -\varepsilon$.
Step 8: Repeat:
8.1: Update clustering center $c_i^{(iter)}$ using (26).
8.2: Update membership matrix $u_{ij}^{(iter)}$ using (25).
8.3: Compute objective function $J^{(iter)}$ using (13) to (15).
8.4: check if $\left|J^{(iter)} - J^{(iter-1)}\right| \leq \varepsilon$ or $iter > iter_{max}$. If yes, then go to step 9; otherwise, let $iter = iter + 1$ and return to step 8.
Step 9: Apply each pixel to the cluster with the highest membership degree and merge subclasses from the same class to obtain the final segmentation result I_{output}.

OUTPUT: I_{output}.

IV. EXPERIMENT AND ANALYSIS

A. EXPERIMENT SETTINGS

To test the robustness of the algorithm to noise, three different types of noise are added to the test images: additive Gaussian noise, salt-and-pepper noise, and uniformly distributed multiplicative noise. The images containing $d\%$ mixed noise are defined as those where additive Gaussian noise with a mean of zero and variance d, salt-and-pepper noise with an intensity of $d\%$, and uniformly distributed multiplicative noise with an intensity of $d\%$ are simultaneously applied to the images.

The proposed algorithm is tested on both synthetic and real images and compared with other algorithms. The algorithms involved in the comparison are: FCM [17], CGFFCM [50], SPFCM [45], FCM_SICM [35], eSFCM [27], SSPFCM [26], and SSFCSC [51]. All the experimental images are subjected to 1%, 5%, 10%, 15%, 20%, and 25% mixed noise. The parameters for the participating algorithms are set as follows: the common parameters for the maximum number of iterations $\text{iter}_{\max}$, the minimum error, and the fuzziness coefficient m are set to 100, 1×10^{-6}, and 2, respectively. For CGFFCM, p_{int}, p_{step}, and $p_{\max}$ are set to 0, 0.1, and 0.5, respectively. For SPFCM, morphological element radius and local window size are both set to 3. Geometric extension σ_d and photometric extension σ_r are set to 5 and 2.5 for FCM_SICM, respectively. For eSFCM, supervision intensity λ is set to 0.5. For SSPFCM, importance to probability memberships a, importance to typicality memberships b,and trade-off coefficient α are all set to 1, coefficients controlling the fuzziness of the typicality values η is set to 2. The controlling parameter α is set to 0.9 for SSFCSC.

The experimental results are evaluated and compared using the segmentation accuracy(SA), mean intersection-over-union(MIOU), peak signal-to-noise ratio (PSNR), and adjusted rand index (ARI).

SA is defined as the ratio of correctly segmented pixels to the total number of pixels. The higher this value, the more pixels have been correctly segmented. Its expression is as follows:

$$\text{SA} = \sum_{i=1}^{k} \frac{R_i \bigcap C_i}{\sum_{j=1}^{k} C_j} \quad (27)$$

where k is the total number of classes; r_i is the set of pixels belonging to the ith class in the segmentation result; and c_i is the set of pixels belonging to the ith class in the ground truth.

MIOU is defined as the average ratio of the intersection and union of the segmentation results and algorithm ground truth across all classes:

$$\text{MIOU} = \frac{1}{k} \sum_{i=1}^{k} \frac{R_i \bigcap C_i}{R_i \bigcup C_i} \quad (28)$$

where all variables are the same as in the above equation.

PSNR can be used to measure the difference between two images. For two images with N pixels, PSNR can be calculated using the following formula:

$$\text{PSNR} = 10 \cdot \log_{10}\left(\frac{\text{MAX}^2}{\text{MSE}}\right) \quad (29)$$

where MAX is the maximum possible pixel value of the images, and MSE (Mean Squared Error) is given by:

$$\text{MSE} = \frac{1}{N} \sum_{i=1}^{N} (I_1(i) - I_2(i))^2 \quad (30)$$

where $I_1(i)$ and $I_2(i)$ are the pixel values of the two images being compared.

ARI is a statistical metric used to measure the similarity between two groupings or clusters. It is based on the Rand Index (RI) but is adjusted to reduce the impact of random

partitioning. The ARI is computed using the following formula:

$$\mathrm{ARI} = \frac{\sum_{ij}\binom{n_{ij}}{2} - \left[\sum_i \binom{a_i}{2}\sum_j \binom{b_j}{2}\right]/\binom{n}{2}}{\frac{1}{2}\left[\sum_i \binom{a_i}{2} + \sum_j \binom{b_j}{2}\right] - \left[\sum_i \binom{a_i}{2}\sum_j \binom{b_j}{2}\right]/\binom{n}{2}} \tag{31}$$

where n is the total number of data points. n_{ij} represents the number of data points common to the i-th cluster of the first partition and the j-th cluster of the second partition. a_i is the total number of elements in the i-th cluster of the first partition, and b_j is the total number of elements in the j-th cluster of the second partition. $\binom{x}{2}$ represents the binomial coefficient. The ARI ranges from $[-1, 1]$, where a value of 1 indicates that the two partitions are perfectly identical, zero means that the similarity is comparable to random partitioning, and negative values indicate that the similarity between the partitions is lower than that of random partitioning.

Normalized Mutual Information (NMI) is another effective metric for evaluating clustering performance. It quantifies the agreement between the clustering results and the ground truth by measuring the amount of mutual information shared, normalized by the entropy of the two distributions. NMI is defined as:

$$\mathrm{NMI} = \frac{2\mathrm{MI}(I_1, I_2)}{\mathrm{H}(I_1) + \mathrm{H}(I_2)} \times 100 \tag{32}$$

where I_1 and I_2 are two datasets of the same size, typically representing the ground truth labels and the clustering results. $MI(I_1, I_2)$ denotes the mutual information between I_1 and I_2, which quantifies the amount of information shared between the two datasets. $H(I_1)$ and $H(I_2)$ represent the entropy of I_1 and I_2, respectively, which measure the uncertainty or variability within each dataset. NMI values range from 0 to 1, where a higher value indicates better clustering performance.

In addition, the Fuzzy Partition Coefficient (V_{pc}) and Fuzzy Partition Entropy (V_{pe}) are widely utilized to assess the efficacy of fuzzy clustering. However, these metrics rely on the dimensions of the membership matrix. Since the proposed algorithm adjusts the number of target clusters during the pre-clustering process, it does not guarantee consistent membership matrix dimensions between the proposed algorithm and comparative algorithms. As a result, V_{pc} and V_{pe} are unsuitable for direct comparisons with other algorithms. Therefore, these metrics are excluded as evaluation metrics in the following experiments.

B. RESULT FOR SYNTHETIC IMAGE WITH MIXED NOISE

Fig. 7 and Fig. 8 illustrate the experimental results of different algorithms on two synthetic images. Both images have a size of 256 × 256 pixels. Synthetic Image 1 (Sy1) is segmented into two categories, while Synthetic Image 2 (Sy2) is segmented into three categories. Tables 1-5 present the segmentation performance of various algorithms evaluated using the following metrics: SA, MIOU, PSNR, ARI and NMI.

From Tables 1-5, with a focus on the Sy1 experimental outcomes, it can be observed that all algorithms perform relatively well under 1% low noise. Notably, SPFCM demonstrates superior performance, with MIOU and PSNR reaching 99.98% and 38.69 dB, respectively. This is attributed to SPFCM's use of morphological methods for effective noise removal and preservation of image details. When processing Sy1 with 1% mixed noise, the PSNR values of the proposed algorithm and FCM_SICM are 25.36 dB and 25.91 dB, respectively, while other algorithms exceed 30 dB. This is because these algorithms consider spatial information but struggle to maintain edge fidelity in the presence of noise. As noise increases, all algorithms experience performance degradation, with FCM and eSFCM showing the most significant decline. When noise reaches 20%, the PSNR values of FCM and eSFCM drop to 8.19 dB and 8.18 dB, respectively, as they rely solely on pixel color and disregard other influencing factors. Similarly, CGFFCM, SSPFCM, and SSFCSC are heavily affected by noise, resulting in significant decreases in segmentation accuracy, PSNR, and ARI. In contrast, SPFCM, FCM_SICM, and the proposed algorithm produce larger homogeneous regions. SPFCM

$$\begin{aligned}
&\frac{\partial J_\lambda}{\partial c_i} = 0 \\
&\Rightarrow 2\sum_{j=1}^{N}\left(1 - A_{ij}\right) {u_{ij}}^2 \left[\alpha\left(c_i - x_j\right) + \beta\left(c_i - \bar{x}_j\right)\right] \\
&\quad + 2\sum_{j=1}^{N} A_{ij}\left(u_{ij} - F_{ij}\right)^2 \left[\alpha\left(c_i - x_j\right) + \beta\left(c_i - \bar{x}_j\right)\right] = 0 \\
&\Rightarrow c_i = \frac{\sum_{j=1}^{N}\left\{\left(1 - A_{ij}\right) {u_{ij}}^2 \left(\alpha x_j + \beta c_i\right) + A_{ij}\left(u_{ij} - F_{ij}\right)^2 \left[\alpha\left(c_i - x_j\right) + \beta\left(c_i - \bar{x}_j\right)\right]\right\}}{(\alpha + \beta)\sum_{j=1}^{N}\left[\left(1 - A_{ij}\right) {u_{ij}}^2 + A_{ij}\left(u_{ij} - F_{ij}\right)^2\right]}
\end{aligned} \tag{26}$$

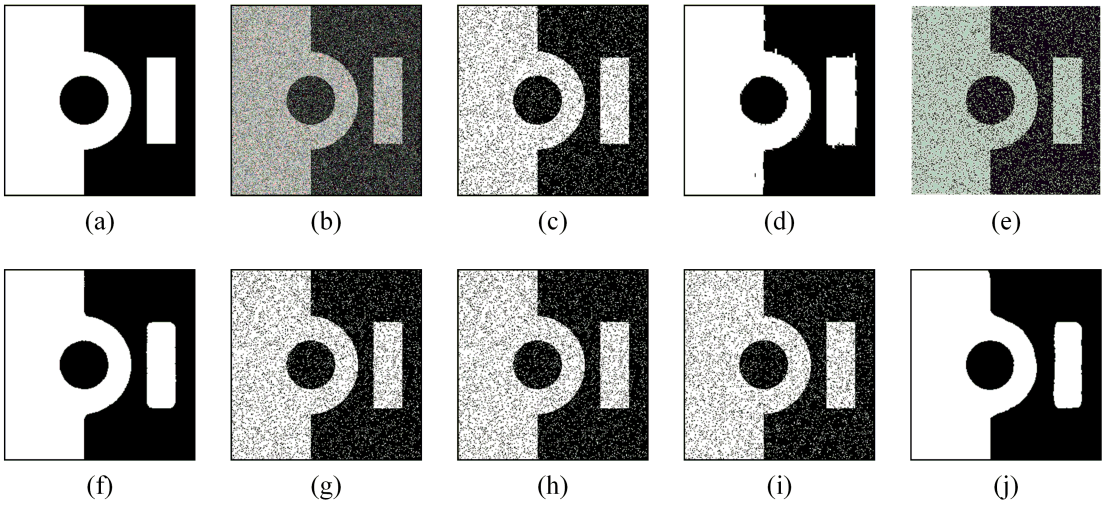

FIGURE 7. The segmentation result of sy1. (a) Original image. (b) Image contaminated with 15% mixed noise. (c)FCM. (d)SPFCM. (e)CGFFCM. (f)FCM_SICM. (g)eSFCM. (h)SSPFCM. (i)SSFCSC. (j) The proposed algorithm.

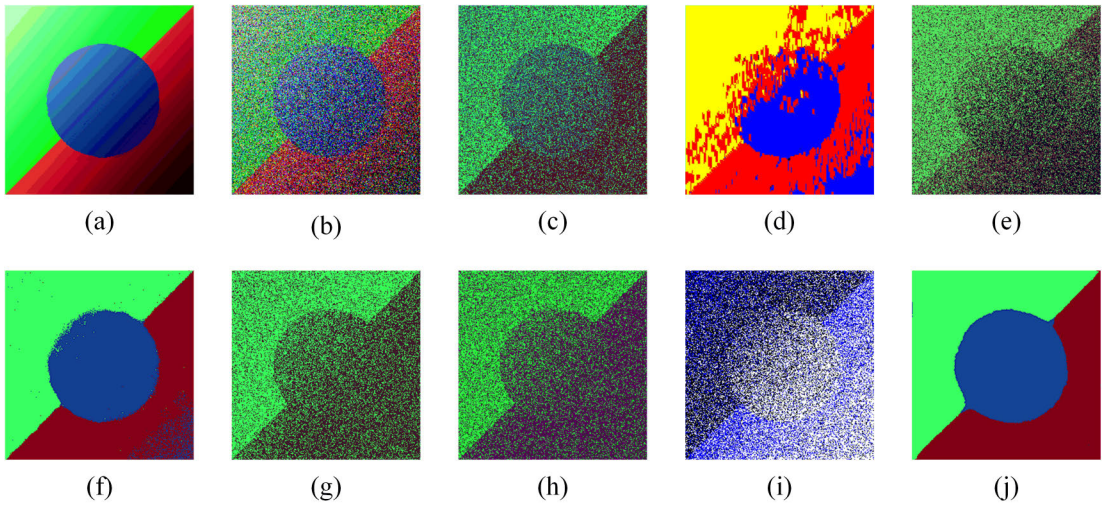

FIGURE 8. The segmentation result of sy2. (a) Original image. (b) Image contaminated with 15% mixed noise. (c)FCM. (d)SPFCM. (e)CGFFCM. (f)FCM_SICM. (g)eSFCM. (h)SSPFCM. (i)SSFCSC. (j) The proposed algorithm.

performs well under low noise levels, while FCM_SICM and the proposed algorithm achieve comparable results. Although they lag slightly behind SPFCM under low noise, their performance remains stable as noise increases. This stability is due to their consideration of spatial information, enabling the correction of noise-contaminated pixels by leveraging neighboring pixel values. Fig. 7 illustrates the segmentation results of various algorithms on Synthetic Image 1 with 15% mixed noise. The results from FCM, CGFFCM, eSFCM, SSPFCM, and SSFCSC are heavily affected by noise, resulting in low-quality segmentation. In contrast, SPFCM, FCM_SICM, and the proposed algorithm produce larger homogeneous regions. However, the segmentation results of SPFCM display discontinuous edges, as shown in Fig. 7(d). This results in PSNR and NMI values of 16.69 dB and 92.33%, respectively, values that are surpassed by the proposed algorithm, achieving 24.17 dB and 97.06%.

From the Sy2 experiment results in Tables 1-5, it is evident that, except for the proposed method, all algorithms experience notable performance deterioration even under minimal noise levels. For instance, while SPFCM achieves a PSNR of 38.69 dB when processing Sy1 with 1% noise, its performance drops drastically to 18.36 dB when processing Sy2. This is because Sy2 is a non-uniform image where each class exhibits a degree of color gradient, with the brightness in the upper-left corner being higher than in the lower-right corner, thereby greatly complicating the segmentation process. As shown in Fig. 8(d) and 8(f), SPFCM and FCM_SICM exhibit comparable noise

TABLE 1. Comparison of SA(%) of different methods on two synthetic images corrupted by different mixed noise.

Images	Noise	FCM	CGFFCMM	SPFCM	FCM_SICM	eSFCM	SSPFCM	SSFCSC	Ours
sy1	1%	99.96	99.52	**99.98**	99.89	99.94	98.34	98.63	99.21
	5%	98.98	96.87	99.76	**99.77**	98.11	97.75	97.25	99.66
	10%	95.46	92.33	99.32	**99.59**	94.38	93.22	95.35	99.41
	15%	90.12	89.72	97.88	98.69	89.68	88.56	91.22	**98.77**
	20%	84.85	81.48	96.31	98.74	78.36	85.23	83.25	**98.87**
	25%	69.21	76.22	95.75	**99.23**	67.85	83.49	82.58	94.94
sy2	1%	97.63	67.62	96.32	97.49	95.37	97.58	92.36	**99.02**
	5%	85.31	60.46	90.17	97.63	76.23	82.35	80.02	**98.64**
	10%	65.33	54.36	82.36	97.11	68.11	71.26	52.36	**98.63**
	15%	58.31	51.34	68.28	96.47	63.31	64.32	51.11	**98.33**
	20%	35.62	49.81	40.32	97.42	37.12	40.27	40.33	**98.39**
	25%	35.66	44.62	42.35	95.33	30.34	37.22	34.25	**97.33**
Mean		76.37	72.03	84.07	98.11	74.90	78.30	74.89	**98.40**
Variance		23.44	19.87	21.96	1.43	23.04	21.21	23.60	**1.25**

TABLE 2. Comparison of MIOU(%) of different methods on two synthetic images corrupted by different mixed noise.

Images	Noise	FCM	CGFFCM	SPFCM	FCM_SICM	eSFCM	SSPFCM	SSFCSC	Ours
sy1	1%	99.97	99.48	**99.98**	99.48	99.92	98.25	98.01	99.38
	5%	97.98	96.68	**99.59**	99.47	97.62	97.22	96.51	98.55
	10%	91.29	91.62	99.14	**99.36**	90.21	92.34	94.32	98.61
	15%	81.99	81.71	97.31	98.39	81.62	85.61	82.02	**98.58**
	20%	73.67	80.56	95.22	98.19	73.58	83.33	81.25	**98.56**
	25%	66.63	75.23	92.21	**98.93**	62.35	81.42	72.84	92.77
sy2	1%	95.49	64.77	96.14	94.89	92.88	95.33	89.36	**98.27**
	5%	81.36	57.35	86.75	95.51	72.36	78.34	77.32	**97.43**
	10%	62.81	52.21	78.36	94.11	65.33	70.39	49.25	**97.39**
	15%	40.07	43.84	62.82	92.91	42.96	45.09	40.08	**96.81**
	20%	31.73	48.33	35.01	94.74	30.36	36.11	35.56	**97.45**
	25%	31.94	43.75	39.37	93.36	25.32	35.24	36.21	**96.19**
Mean		71.24	69.63	81.83	96.61	69.54	74.89	71.06	**97.50**
Variance		25.09	20.60	23.49	2.58	25.44	23.34	24.17	**1.74**

TABLE 3. Comparison of PSNR(dB) of different methods on two synthetic images corrupted by different mixed noise.

Images	Noise	FCM	CGFFCM	SPFCM	FCM_SICM	eSFCM	SSPFCM	SSFCSC	Ours
sy1	1%	38.62	36.78	**38.69**	25.91	38.12	32.25	30.25	25.36
	5%	19.94	17.36	**28.59**	25.83	20.36	20.36	21.22	24.08
	10%	13.43	13.59	21.36	**25.01**	13.47	14.32	15.75	24.19
	15%	10.05	9.98	16.96	**25.17**	9.96	9.73	10.06	24.17
	20%	8.19	9.79	11.23	23.94	8.18	9.25	8.35	**24.09**
	25%	6.98	8.96	10.33	**22.72**	7.01	9.03	7.96	20.24
Sy2	1%	21.12	12.23	18.36	18.09	16.93	17.32	17.33	**26.81**
	5%	12.21	10.36	15.35	18.98	12.36	14.25	12.89	**22.14**
	10%	8.89	8.22	12.71	17.51	9.33	10.27	8.52	**21.82**
	15%	6.57	6.91	9.66	17.73	6.81	5.84	5.86	**22.77**
	20%	6.44	7.25	6.41	17.54	6.57	6.31	5.18	**22.35**
	25%	6.92	6.98	6.44	16.63	5.27	6.21	5.02	**19.34**
Mean		13.28	12.37	16.34	21.26	12.86	12.93	12.37	**23.11**
Variance		9.42	8.27	9.52	3.79	9.16	7.61	7.62	**2.10**

robustness to their performance on Sy1. However, their segmentation results for Sy2 display under-segmentation in the lower-right corner of the image. This issue arises because the lower-right corner's lower brightness is easily

TABLE 4. Comparison of ARI of different methods on two synthetic images corrupted by different mixed noise.

Images	Noise	FCM	CGFFCM	SPFCM	FCM_SICM	eSFCM	SSPFCM	SSFCSC	Ours
sy1	1%	0.9996	0.9826	**0.9998**	0.9902	0.9995	0.9836	0.9836	0.9894
	5%	0.9607	0.8714	0.9903	**0.9909**	0.9624	0.9677	0.9634	0.9842
	10%	0.8258	0.7211	0.9833	**0.9871**	0.8212	0.8631	0.8122	0.9771
	15%	0.6432	0.5432	0.9425	**0.9863**	0.6434	0.7132	0.6478	0.9738
	20%	0.4805	0.3913	0.9223	0.9823	0.4736	0.5365	0.3428	**0.9828**
	25%	0.3531	0.2817	0.9114	**0.9788**	0.0321	0.3636	0.2875	0.9236
sy2	1%	0.9362	0.4922	0.9132	0.9265	0.8992	0.9632	0.8352	**0.9763**
	5%	0.5883	0.3453	0.8611	0.9305	0.3331	0.6726	0.4722	**0.9617**
	10%	0.3082	0.1593	0.8235	0.9297	0.2790	0.3666	0.3562	**0.9578**
	15%	0.1301	0.1434	0.3522	0.9247	0.1206	0.1786	0.1863	**0.9631**
	20%	0.0812	0.0993	0.1532	0.9224	0.0195	0.1128	0.1112	**0.9555**
	25%	0.0653	0.0557	0.1985	0.9172	0.0615	0.0628	0.0856	**0.9447**
Mean		0.5310	0.4241	0.7543	0.9556	0.4704	0.5654	0.5070	**0.9655**
Variance		0.3484	0.3067	0.3205	0.0321	0.3813	0.3444	0.3292	**0.0186**

TABLE 5. Comparison of NMI(%) of different methods on two synthetic images corrupted by different mixed noise.

Images	Noise	FCM	CGFFCM	SPFCM	FCM_SICM	eSFCM	SSPFCM	SSFCSC	Ours
sy1	1%	99.93	97.59	**99.96**	98.69	99.12	97.58	98.01	98.52
	5%	95.95	54.63	98.81	**98.78**	95.87	96.17	95.32	97.98
	10%	80.32	72.03	98.10	**98.52**	85.72	85.93	80.12	97.51
	15%	92.11	53.23	92.33	**98.17**	61.24	70.05	62.32	97.06
	20%	41.25	37.86	91.41	98.32	44.74	52.36	34.25	**98.37**
	25%	32.82	27.69	89.85	**96.73**	5.22	34.52	25.71	91.75
sy2	1%	91.36	48.23	90.37	91.58	88.35	95.33	80.37	**96.99**
	5%	55.17	33.34	86.42	91.75	31.88	65.82	46.52	**96.01**
	10%	28.36	15.62	81.75	91.02	25.06	35.36	34.92	**95.32**
	15%	12.25	14.36	34.43	91.08	11.52	15.75	17.34	**95.93**
	20%	8.05	9.83	14.31	90.45	3.51	11.25	11.02	**94.78**
	25%	6.33	5.22	17.26	89.82	5.77	5.98	8.03	**93.85**
Mean		51.16	41.64	74.58	94.58	46.50	55.51	49.49	**96.17**
Variance		34.80	30.33	32.46	3.85	37.93	34.51	32.70	**2.01**

TABLE 6. Comparison number of iteration steps of different methods on two synthetic images corrupted by different mixed noise.

Images	Noise	FCM	CGFFCM	SPFCM	FCM_SICM	eSFCM	SSPFCM	SSFCSC	Ours
sy1	1%	9	38	32	7	18	10	11	9
	5%	10	42	37	9	25	10	11	9
	10%	12	51	38	8	46	12	13	9
	15%	16	51	40	8	100	17	12	8
	20%	15	53	39	9	100	15	13	10
	25%	20	53	43	8	100	15	15	12
sy2	1%	23	69	100	21	57	12	18	20
	5%	25	52	100	14	68	13	21	21
	10%	64	57	100	22	83	17	20	21
	15%	89	52	100	16	75	14	17	21
	20%	60	55	100	13	100	21	22	20
	25%	58	52	100	14	100	19	25	21
Mean		33	52	69	12	73	15	17	15

confused with the dark circular region in the center of the image, resulting in segmentation inaccuracies. The proposed algorithm addresses this challenge by refining clusters, segmenting the darker regions into a distinct cluster. It also

employs label propagation to differentiate the supervised information of pixels in the lower-right corner from those within the central circle, effectively distinguishing the two regions. Consequently, this markedly enhances segmentation outcomes, as illustrated in Fig. 8(j). When segmenting Sy2, the proposed algorithm achieves an average MIOU and ARI of 22.53 dB and 0.9599, respectively, outperforming SPFCM's 11.48 dB and 0.5502 and FCM_SICM's 17.74 dB and 0.9251. The experimental data demonstrate that the proposed method, through cluster refinement, label propagation, and adaptive weighting of local spatial information, effectively overcomes the challenges of segmenting noisy images.

The number of iterations is also a key metric for assessing algorithm efficiency. Table 6 presents the iteration counts of the compared algorithms. The data indicate that the number of iterations generally increases with noise density. SPFCM and eSFCM require significantly more iterations, frequently hitting the iteration limit when processing Sy2 or high-noise images. CGFFCM maintains a consistent iteration count of approximately 60 by dynamically adjusting the power of the cluster weight vector during the iteration process. FCM_SICM, on the other hand, completes clustering with substantially fewer iterations, as it leverages a membership linkage mechanism to incorporate information from previous iterations. This mechanism enables FCM_SICM to achieve clustering within 30 iterations in most cases. The proposed SSFCM-LP algorithm achieves efficient clustering through the effective use of supervised information to guide the process. It eliminates the need for complex parameters or computations during the iterative process and replaces the random initialization of the membership matrix with results from label propagation. This results in fewer, more stable iterations while also reducing the likelihood of getting stuck in local optima.

C. RESULT FOR NATURAL IMAGE WITH MIXED NOISE

Natural images often exhibit variations in illumination, noise interference, and complex backgrounds. Illumination variation refers to changes in light intensity and direction within an image, which can influence the visibility and color perception of objects. Noise interference involves the introduction of unwanted random signals, often leading to blurred details. Complex backgrounds, characterized by diverse and chaotic elements, complicate the recognition and segmentation of target objects. The segmentation results on natural images provide a more comprehensive assessment of an algorithm's performance. In this section, various algorithms are used to perform segmentation tests on images from the Berkeley dataset [48], and the proposed algorithm is also tested on images from the MSRC [52] and AID [53] datasets. All images are subjected to 10% mixed noise, and the experimental results show the best outcomes in 10 trials.

As shown in Fig. 9, the segmentation results of FCM, CGFFCM, and eSFCM are severely affected by noise, rendering the segmented targets indistinguishable. Although the SPFCM algorithm demonstrates good performance in synthetic image experiments, its efficacy diminishes when applied to natural images with more complex and diverse features. This is because SPFCM is based on grayscale reconstruction, which struggles to process complex and irregular regions effectively. When segmenting images #124084 and #208001, SPFCM can identify the main objects but struggles to form accurate homogeneous regions. SSPFCM achieves superior segmentation of main regions relative to FCM due to the guidance provided by semi-supervised information, which reduces the impact of noise. However, the segmentation results remain significantly impacted by noise. FCM_SICM performs well in segmenting color images but demonstrates errors in processing images like #12003, #124084, and #299091. For instance, in image #12003, it cannot differentiate between the starfish and the light-colored parts of the background. Similarly, in image #124084, parts of the flower's stamens are mistakenly classified as part of the background. The proposed algorithm demonstrates robustness against noise, with no contamination observed in the segmentation results. Additionally, by fully leveraging semi-supervised information and refining clusters, the proposed algorithm performs exceptionally well in processing complex and non-uniform images. For example, when processing image #124084, it correctly segments the background with highly uneven illumination, highlighting its advanced capability in addressing difficult conditions.

Fig. 10 and Fig. 11 show the segmentation results of the proposed algorithm on color images from the MSRC dataset and remote sensing images from the AID dataset, respectively. The first row displays the original images, the second row shows the images with 10% mixed noise added, and the third row presents the segmentation results of the proposed algorithm.

Fig. 10 presents the segmentation results of the proposed algorithm on six images from the MSRC dataset, each with a size of 320 $\times$ 240 pixels. From the figure, it is evident that the proposed algorithm forms continuous regions in the segmentation of MSRC dataset images, though some edge details are lost. For example, the green tree image loses the edge details of the leaves, and in the two images containing cows, the algorithm can locate the cows, but the edges are not accurately delineated. However, in the images of the signpost and plastic chair, the segmentation results are excellent; the text on the signpost and the texture of the tiles on the ground behind the plastic chair do not adversely affect the algorithm's performance.

Fig. 11 displays the segmentation results of the proposed algorithm on six remote sensing images from the AID dataset, each sized 600 $\times$ 600 pixels, covering categories such as lakes, forests, bridges, and buildings. In the segmentation

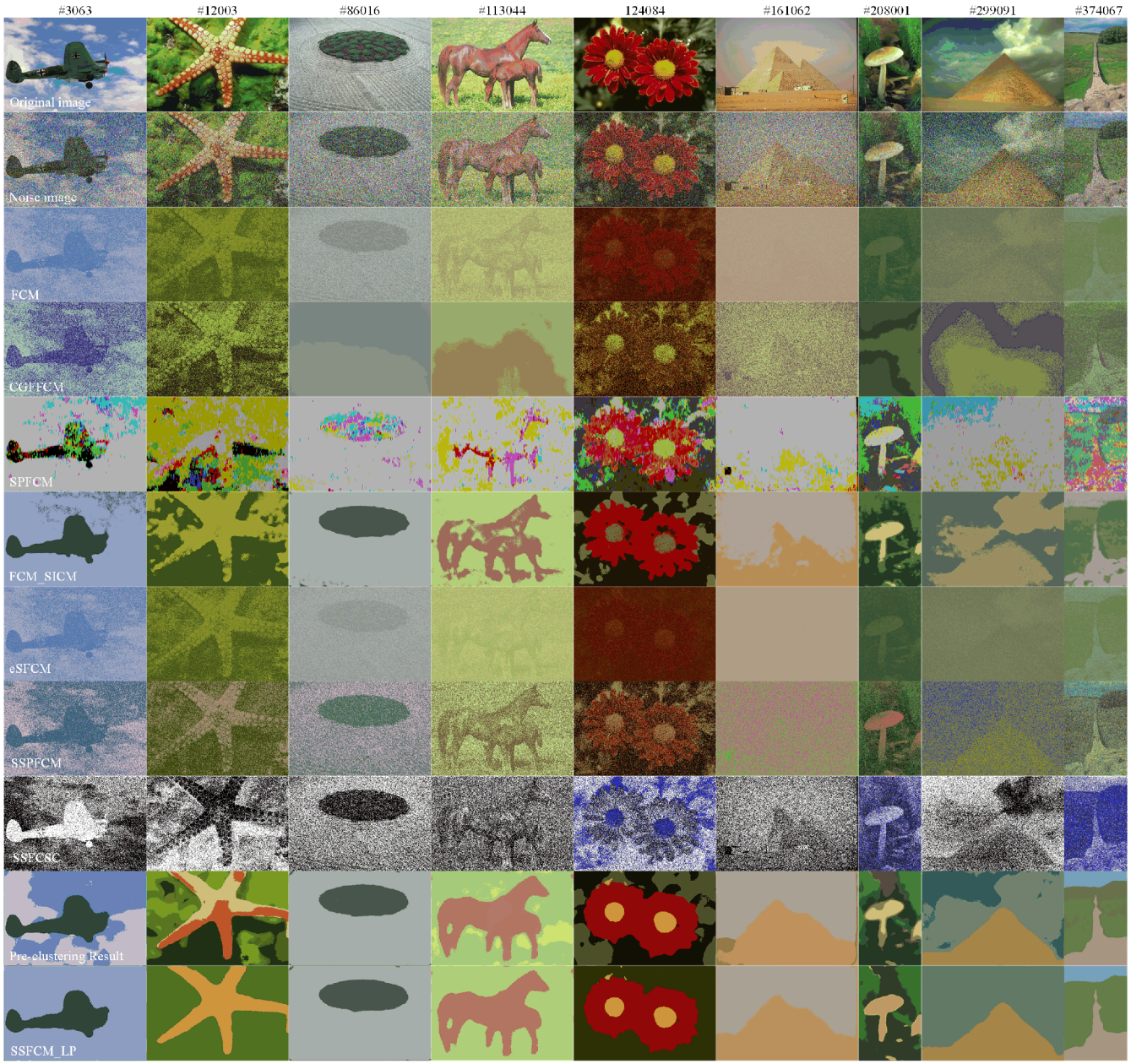

FIGURE 9. Segmentation results of images from the Berkeley database by different algorithms.

results of the bridge image in the first column, the algorithm accurately segments the main body of the bridge; however, due to the very similar colors of the river and the riverbank, some segmentation errors occur. When segmenting the road image in the fifth column, noise causes the algorithm to fail in extracting some of the finer roads. The other images achieve relatively ideal segmentation results. Notably, the accurate results for the pond in the third column and the stadium in the sixth column are due to the effectiveness of pre-clustering, as the pond's color closely resembles that of the bank below, and the stadium image has significant light and shadow variations. In summary, the proposed algorithm achieves more accurate segmentation across various types of color images.

D. ANALYSIS OF COMPUTATIONAL COMPLEXITY

Algorithmic complexity serves as a critical metric when comparing algorithms. This section calculates and compares the computational complexities of various clustering segmentation algorithms, presenting the average runtime for processing synthetic images with varying levels of mixed noise, as discussed in Section IV-B.

As illustrated in the Table 7, N represents the total number of pixels in the image, k denotes the number of clusters,

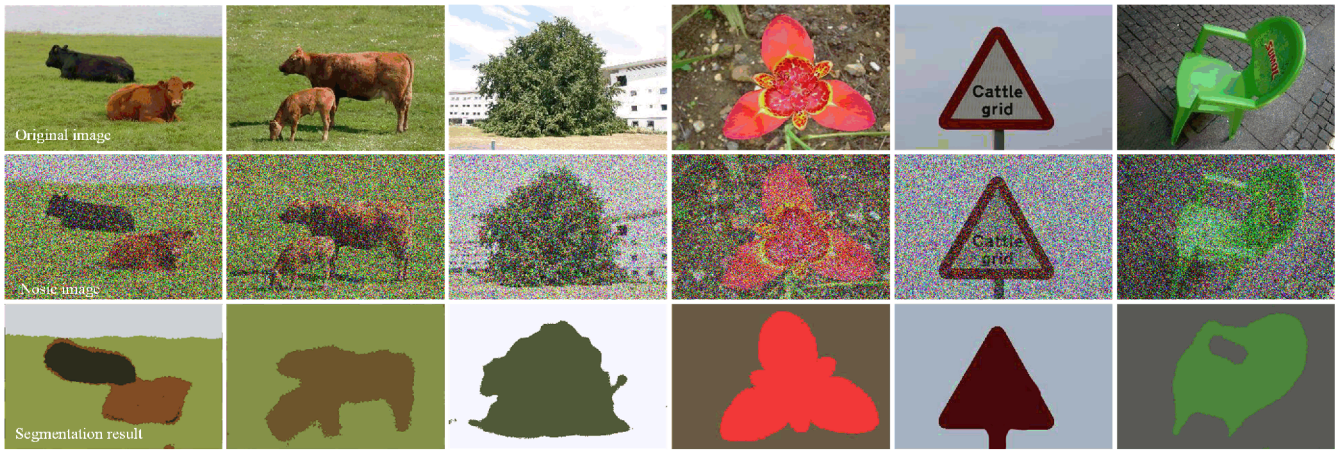

FIGURE 10. Segmentation results of the proposed algorithm for images from the MSRC database.

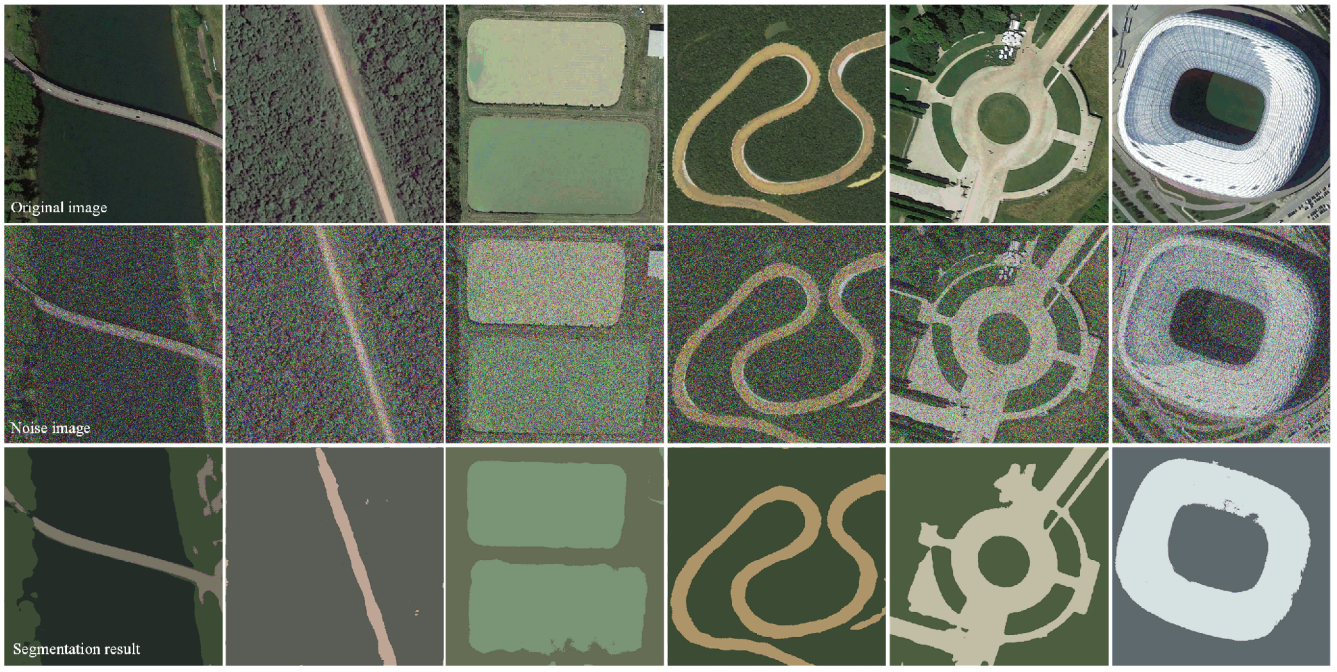

FIGURE 11. Segmentation results of the proposed algorithm for images from the AID database.

TABLE 7. Complexity analysis and average running time for synthetic images with different mixed noise.

Methods	Numbers of computational steps	Average runtime for synthetic images(s)
FCM	$N \times k \times T$	0.23
CGFFCM	$T \times (NMk + NMk + NMk + NMk)$	3.72
SFFCM	$L \times N \times h^2 + N \times k \times T$	0.31
FCM_SICM	$N_D \times Q_D \times \log_2(N_D \times Q_D) + N + (N + N) \times K \times T$	0.15
eSFCM	$N \times k \times T$	0.47
SSPFCM	$N \times M \times k \times T$	0.26
SSFCSC	$N \times k \times T$	0.48
Ours	$N_D \times Q_D \times \log_2(N_D \times Q_D) + (N - l) \times l \times k + l^2 + N \times \tilde{k} \times T$	0.33

and T signifies the number of iterations. In the CGFFCM and SSPFCM algorithms, M denotes the number of features. For the SFFCM algorithm, h denotes the side length of the neighborhood window, and L signifies the number of

intensity levels in the image. In the FCM_SICM and our proposed algorithm, the computational steps of the bilateral filter are expressed as $N_D \times Q_D \times \log_2(N_D \times Q_D)$. Additionally, l denotes the number of semi-supervised labeled pixels, while $\tilde{k}$ signifies the number of subclasses.

In terms of runtime, most algorithms demonstrate comparable time expenditures. The FCM_SICM algorithm decreases the number of iterations through a membership connectivity mechanism, thereby resulting in shorter runtimes. Our proposed algorithm initializes the membership matrix with semi-supervised information, further decreasing runtime. Although SPFCM and eSFCM require more iterations to achieve convergence, their lower complexity during the iterative process results in relatively short runtimes. In contrast, the CGFFCM algorithm requires significantly longer runtimes.

This section discusses the advantages and disadvantages of the proposed algorithm compared to other algorithms. First, compared with basic FCM and semi-supervised FCM algorithms, the FCM and eSFCM algorithms do not consider information beyond pixel color, resulting in simpler iterative formulas and faster running speeds than the proposed algorithm. However, they are severely affected by noise. Second, compared with algorithms that use morphological methods for noise suppression, SPFCM combines wavelet decomposition and reconstruction with morphological methods to suppress noise. In simple images dominated by straight lines and arcs in binary and edge representations, morphological methods can effectively remove noise while preserving edges. However, in color and natural images, performance of the SPFCM is inferior to that of the proposed algorithm. Third, CGFFCM, a method based on multi-feature weighting, accounts for multiple image attributes such as color, texture, and gradient. However, it has a longer running time than the proposed algorithm and is not as effective in suppressing noise. Fourth, compared with the FCM_SICM algorithm, which also utilizes local spatial information, the proposed algorithm exhibits similar robustness. FCM_SICM accelerates convergence using membership linking, whereas the proposed algorithm uses a label matrix to initialize the membership matrix, thereby accelerating convergence. When processing color images, the proposed algorithm refines clusters using semi-supervised information, ensuring more uniformity within each class by employing a perceptually uniform color system, resulting in higher accuracy in natural image segmentation. Finally, other semi-supervised FCM algorithms are considered. Merely using semi-supervised information is insufficient to suppress noise, and when the semi-supervised information is contaminated by noise, the clustering process can be severely misled, leading to a significant decline in segmentation performance with increased noise. Additionally, except for FCM_SICM and the proposed algorithm, the above algorithms require parameter selection during clustering and lack adaptability and flexibility. Compared with the aforementioned algorithms, the proposed algorithm enhances operability and adaptability to different images while ensuring segmentation accuracy for color and natural images.

V. CONCLUSION

To address the poor noise performance and insufficient use of semi-supervised information in current semi-supervised FCM algorithms, we proposed an adaptive semi-supervised FCM segmentation algorithm that uses pre-clustering with semi-supervised learning and incorporates local spatial information. First, the algorithm refines clusters using semi-supervised information to ensure more uniform data within each class and employs a perceptually uniform color system. Second, the algorithm propagates labels within the supervision matrix and introduces the concept of a supervised center, thereby ensuring the full utilization of semi-supervised information. Finally, the objective function includes two sets of adaptive parameters to control the intensity of semi-supervised and spatial information.

Experiments demonstrate that the proposed algorithm performs well in noisy environments and shows significant advantages in processing color images. However, the algorithm exhibits certain limitations: in images heavily affected by noise, it struggles to effectively preserve edge details. Even in images with minimal noise, distortion of edge information may still occur. Although the algorithm can enhance clustering accuracy with a small amount of supervised information, the necessity to iterate through supervised pixels for parameter computation leads to a substantial increase in runtime as the amount of supervised information grows, thereby reducing the efficiency of information utilization. The challenges of maintaining edge information and efficiently leveraging large quantities of supervised information require further exploration. Additionally, intuitionistic fuzzy logic, known for its flexibility in handling uncertain and complex decision-making problems, presents a promising avenue for enhancing FCM image segmentation algorithms and merits further investigation.

REFERENCES

[1] M. Amiriebrahimabadi, Z. Rouhi, and N. Mansouri, "A comprehensive survey of multi-level thresholding segmentation methods for image processing," *Arch. Comput. Methods Eng.*, vol. 31, no. 6, pp. 3647–3697, Mar. 2024.

[2] S. Pare, A. Kumar, G. K. Singh, and V. Bajaj, "Image segmentation using multilevel thresholding: A research review," *Iranian J. Sci. Technol., Trans. Electr. Eng.*, vol. 44, no. 1, pp. 1–29, Mar. 2020.

[3] C. J. J. Sheela and G. Suganthi, "Morphological edge detection and brain tumor segmentation in magnetic resonance (MR) images based on region growing and performance evaluation of modified fuzzy C-means (FCM) algorithm," *Multimedia Tools Appl.*, vol. 79, nos. 25–26, pp. 17483–17496, Jul. 2020.

[4] J. Jing, S. Liu, G. Wang, W. Zhang, and C. Sun, "Recent advances on image edge detection: A comprehensive review," *Neurocomputing*, vol. 503, pp. 259–271, Sep. 2022.

[5] X. Wang, S. Wang, Y. Guo, K. Hu, and W. Wang, "Coal gangue image segmentation method based on edge detection theory of star algorithm," *Int. J. Coal Preparation Utilization*, vol. 43, no. 1, pp. 119–134, Jan. 2023.

[6] C. Chen, C. Wang, B. Liu, C. He, L. Cong, and S. Wan, "Edge intelligence empowered vehicle detection and image segmentation for autonomous vehicles," *IEEE Trans. Intell. Transp. Syst.*, vol. 24, no. 11, pp. 13023–13034, Jan. 2023.

[7] K. Parvati, B. S. Prakasa Rao, and M. Mariya Das, "Image segmentation using gray-scale morphology and marker-controlledWatershed transformation," *Discrete Dyn. Nature Soc.*, vol. 2008, no. 1, Jan. 2008, Art. no. 384346.

[8] D. Chudasama, T. Patel, S. Joshi, and G. I. Prajapati, "Image segmentation using morphological operations," *Int. J. Comput. Appl.*, vol. 117, no. 18, pp. 16–19, May 2015.

[9] S. Carvalho, A. Horovistiz, and J. P. Davim, "Morphological characterization of chip segmentation in Ti-6Al-7Nb machining: A novel method based on digital image processing," *Measurement*, vol. 206, Jan. 2023, Art. no. 112330.

[10] T. Lei, X. Jia, Y. Zhang, S. Liu, H. Meng, and A. K. Nandi, "Superpixel-based fast fuzzy C-means clustering for color image segmentation," *IEEE Trans. Fuzzy Syst.*, vol. 27, no. 9, pp. 1753–1766, Sep. 2019.

[11] H. Mittal, A. C. Pandey, M. Saraswat, S. Kumar, R. Pal, and G. Modwel, "A comprehensive survey of image segmentation: Clustering methods, performance parameters, and benchmark datasets," *Multimedia Tools Appl.*, vol. 81, no. 24, pp. 35001–35026, Oct. 2022.

[12] P. M. M. Pereira, R. Fonseca-Pinto, R. P. Paiva, P. A. A. Assuncao, L. M. N. Tavora, L. A. Thomaz, and S. M. M. Faria, "Dermoscopic skin lesion image segmentation based on local binary pattern clustering: Comparative study," *Biomed. Signal Process. Control*, vol. 59, May 2020, Art. no. 101924.

[13] Y. Miao, S. Li, L. Wang, H. Li, R. Qiu, and M. Zhang, "A single plant segmentation method of maize point cloud based on Euclidean clustering and K-means clustering," *Comput. Electron. Agricult.*, vol. 210, Jul. 2023, Art. no. 107951.

[14] Z. Ning, S. Zhong, Q. Feng, W. Chen, and Y. Zhang, "SMU-Net: Saliency-guided morphology-aware U-Net for breast lesion segmentation in ultrasound image," *IEEE Trans. Med. Imag.*, vol. 41, no. 2, pp. 476–490, Feb. 2022.

[15] S. Minaee, Y. Boykov, F. Porikli, A. Plaza, N. Kehtarnavaz, and D. Terzopoulos, "Image segmentation using deep learning: A survey," *IEEE Trans. Pattern Anal. Mach. Intell.*, vol. 44, no. 7, pp. 3523–3542, Jul. 2022.

[16] Z. Wang, E. Wang, and Y. Zhu, "Image segmentation evaluation: A survey of methods," *Artif. Intell. Rev.*, vol. 53, no. 8, pp. 5637–5674, Dec. 2020.

[17] J. C. Bezdek, R. Ehrlich, and W. Full, "FCM: The fuzzy c-means clustering algorithm," *Comput. Geosci.*, vol. 10, nos. 2–3, pp. 191–203, Jan. 1984.

[18] L. A. Zadeh, "Fuzzy sets," *Inf. Control*, vol. 8, no. 3, pp. 338–353, Jun. 1965.

[19] Y. Qin, S. Ding, L. Wang, and Y. Wang, "Research progress on semi-supervised clustering," *Cognit. Comput.*, vol. 11, no. 5, pp. 599–612, Oct. 2019.

[20] J. Cai, J. Hao, H. Yang, X. Zhao, and Y. Yang, "A review on semi-supervised clustering," *Inf. Sci.*, vol. 632, pp. 164–200, Mar. 2023.

[21] A. Golzari Oskouei, N. Samadi, and J. Tanha, "Feature-weight and cluster-weight learning in fuzzy c-means method for semi-supervised clustering," *Appl. Soft Comput.*, vol. 161, Aug. 2024, Art. no. 111712.

[22] F. Zhao, M. Zhang, and H. Liu, "Multiple population-based multi-objective evolutionary semi-supervised multi-kernel region fuzzy clustering image segmentation," *Memetic Comput.*, vol. 15, no. 4, pp. 451–468, Dec. 2023.

[23] W. Pedrycz, "Algorithms of fuzzy clustering with partial supervision," *Pattern Recognit. Lett.*, vol. 3, no. 1, pp. 13–20, Jan. 1985.

[24] S. Peng, W. Ser, B. Chen, and Z. Lin, "Robust semi-supervised nonnegative matrix factorization for image clustering," *Pattern Recognit.*, vol. 111, Mar. 2021, Art. no. 107683.

[25] N. R. Pal, K. Pal, J. M. Keller, and J. C. Bezdek, "A possibilistic fuzzy C-means clustering algorithm," *IEEE Trans. Fuzzy Syst.*, vol. 13, no. 4, pp. 517–530, Aug. 2005.

[26] H. Yu, X. Xu, H. Li, Y. Wu, and B. Lei, "Semi-supervised possibilistic c-means clustering algorithm based on feature weights for imbalanced data," *Knowl.-Based Syst.*, vol. 286, Feb. 2024, Art. no. 111388.

[27] E. Yasunori, H. Yukihiro, Y. Makito, and M. Sadaaki, "On semi-supervised fuzzy C-means clustering," in *Proc. IEEE Int. Conf. Fuzzy Syst.*, Aug. 2009, pp. 1119–1124.

[28] W. Pedrycz and J. Waletzky, "Fuzzy clustering with partial supervision," *IEEE Trans. Syst., Man, Cybern., B, Cybern.*, vol. 27, no. 5, pp. 787–795, Oct. 1997.

[29] X. Yin, T. Shu, and Q. Huang, "Semi-supervised fuzzy clustering with metric learning and entropy regularization," *Knowl.-Based Syst.*, vol. 35, pp. 304–311, Nov. 2012.

[30] A. M. Bensaid, L. O. Hall, J. C. Bezdek, and L. P. Clarke, "Partially supervised clustering for image segmentation," *Pattern Recognit.*, vol. 29, no. 5, pp. 859–871, May 1996.

[31] T. Finley and T. Joachims, "Supervised k-means clustering," Dept. Comput. Sci., Cornell Univ., Ithaca, NY, USA, Tech. Rep., 2008. [Online]. Available: http://www.cs.cornell.edu/~tomf/publications/supervised_kmeans-08.pdf

[32] T. W. Finley, "Supervised clustering with structural SVMs," Ph.D. thesis, Dept. Comput. Sci., Cornell Univ., Ithaca, NY, USA, 2009.

[33] S. Chen and D. Zhang, "Robust image segmentation using FCM with spatial constraints based on new kernel-induced distance measure," *IEEE Trans. Syst., Man Cybern., B, Cybern.*, vol. 34, no. 4, pp. 1907–1916, Aug. 2004.

[34] S. Krinidis and V. Chatzis, "A robust fuzzy local information C-means clustering algorithm," *IEEE Trans. Image Process.*, vol. 19, no. 5, pp. 1328–1337, May 2010.

[35] Q. Wang, X. Wang, C. Fang, and W. Yang, "Robust fuzzy c-means clustering algorithm with adaptive spatial & intensity constraint and membership linking for noise image segmentation," *Appl. Soft Comput.*, vol. 92, Jul. 2020, Art. no. 106318.

[36] J. Xu, T. Zhao, G. Feng, M. Ni, and S. Ou, "A fuzzy C-means clustering algorithm based on spatial context model for image segmentation," *Int. J. Fuzzy Syst.*, vol. 23, no. 3, pp. 816–832, Apr. 2021.

[37] F. Zhao, L. Jiao, and H. Liu, "Fuzzy c-means clustering with non local spatial information for noisy image segmentation," *Frontiers Comput. Sci. China*, vol. 5, no. 1, pp. 45–56, Mar. 2011.

[38] F. Zhao, "Fuzzy clustering algorithms with self-tuning non-local spatial information for image segmentation," *Neurocomputing*, vol. 106, pp. 115–125, Apr. 2013.

[39] T. Wei, X. Wang, X. Li, and S. Zhu, "Fuzzy subspace clustering noisy image segmentation algorithm with adaptive local variance & non-local information and mean membership linking," *Eng. Appl. Artif. Intell.*, vol. 110, Apr. 2022, Art. no. 104672.

[40] H. Van Lung and J.-M. Kim, "A generalized spatial fuzzy c-means algorithm for medical image segmentation," in *Proc. IEEE Int. Conf. Fuzzy Syst.*, Aug. 2009, pp. 409–414.

[41] X. Jia, T. Lei, X. Du, S. Liu, H. Meng, and A. K. Nandi, "Robust self-sparse fuzzy clustering for image segmentation," *IEEE Access*, vol. 8, pp. 146182–146195, 2020.

[42] X. Li and Z. Qu, "Adaptive spatially weighted fuzzy c-means clustering for image segmentation," in *Proc. 7th Int. Conf. Intell. Comput. Signal Process. (ICSP)*, Apr. 2022, pp. 1920–1923.

[43] R. R. Gharieb, G. Gendy, A. Abdelfattah, and H. Selim, "Adaptive local data and membership based KL divergence incorporating C-means algorithm for fuzzy image segmentation," *Appl. Soft Comput.*, vol. 59, pp. 143–152, Oct. 2017.

[44] J. Gu, L. Jiao, S. Yang, and F. Liu, "Fuzzy double C-means clustering based on sparse self-representation," *IEEE Trans. Fuzzy Syst.*, vol. 26, no. 2, pp. 612–626, Apr. 2018.

[45] C. Wang, W. Pedrycz, M. Zhou, and Z. Li, "Sparse regularization-based fuzzy C-means clustering incorporating morphological grayscale reconstruction and wavelet frames," *IEEE Trans. Fuzzy Syst.*, vol. 29, no. 7, pp. 1826–1840, Jul. 2021.

[46] A. Rodriguez and A. Laio, "Clustering by fast search and find of density peaks," *Science*, vol. 344, no. 6191, pp. 1492–1496, Jun. 2014.

[47] Y. Wang, J. Qian, M. Hassan, X. Zhang, T. Zhang, C. Yang, X. Zhou, and F. Jia, "Density peak clustering algorithms: A review on the decade 2014–2023," *Expert Syst. Appl.*, vol. 238, Mar. 2024, Art. no. 121860.

[48] P. Arbeláez, M. Maire, C. Fowlkes, and J. Malik, "Contour detection and hierarchical image segmentation," *IEEE Trans. Pattern Anal. Mach. Intell.*, vol. 33, no. 5, pp. 898–916, May 2011.

[49] H. Zhang and J. Lu, "Semi-supervised fuzzy clustering: A kernel-based approach," *Knowl.-Based Syst.*, vol. 22, no. 6, pp. 477–481, Aug. 2009.

[50] A. Golzari Oskouei, M. Hashemzadeh, B. Asheghi, and M. A. Balafar, "CGFFCM: Cluster-weight and group-local feature-weight learning in fuzzy C-means clustering algorithm for color image segmentation," *Appl. Soft Comput.*, vol. 113, Dec. 2021, Art. no. 108005.

[51] L. H. Son and T. M. Tuan, "Dental segmentation from X-ray images using semi-supervised fuzzy clustering with spatial constraints," *Eng. Appl. Artif. Intell.*, vol. 59, pp. 186–195, Mar. 2017.
[52] J. Shotton, J. Winn, C. Rother, and A. Criminisi, "TextonBoost: Joint appearance, shape and context modeling for multi-class object recognition and segmentation," in *Proc. 9th Eur. Conf. Comput. Vis.*, Graz, Austria, Jan. 2006, pp. 1–15.
[53] G.-S. Xia, J. Hu, F. Hu, B. Shi, X. Bai, Y. Zhong, L. Zhang, and X. Lu, "AID: A benchmark data set for performance evaluation of aerial scene classification," *IEEE Trans. Geosci. Remote Sens.*, vol. 55, no. 7, pp. 3965–3981, Jul. 2017.

HAO-RAN CHEN received the B.S. degree in communications engineering from Beijing Jiaotong University, in 2022. He is currently pursuing the master's degree with the School of Electronic and Information Engineering, Lanzhou Jiaotong University.

His research interest includes image processing.

XIAO-PENG WANG received the Ph.D. degree from Northwestern Polytechnical University, Xi'an, China, in 2005.

He is currently a Professor and a Doctoral Supervisor with the School of Electronic and Information Engineering, Lanzhou Jiaotong University. His research interest includes image processing and analysis.

JIA-XIN WU is currently pursuing the Ph.D. degree in rail transit communication engineering with the School of Electronic and Information Engineering, Lanzhou Jiaotong University. His research interest includes image processing.

HAI-ZHOU WANG is currently pursuing the master's degree with the School of Electronic and Information Engineering, Lanzhou Jiaotong University. His research interest includes image processing.